Propagation Graph Fusion for Multi-Modal Medical Content-Based Retrieval

Sidong Liu*†, Siqi Liu†, Sonia Pujol*, Ron Kikinis*, Dagan Feng†‡, Weidong Cai†
* Surgical Planning Laboratory, Brigham and Women's Hospital
Harvard Medical School, Boston, MA, USA
† BMIT Research Group, School of Information Technologies
University of Sydney, Sydney, NSW, Australia
‡ Med-X Research Institute, Shanghai Jiaotong University, Shanghai, China

***Abstract*—Medical content-based retrieval (MCBR) plays an important role in computer aided diagnosis and clinical decision support. Multi-modal imaging data have been increasingly used in MCBR, as they could provide more insights of the diseases and complement the deficiencies of single-modal data. However, it is very challenging to fuse data in different modalities since they have different physical fundamentals and large value range variations. In this study, we propose a novel Propagation Graph Fusion (PGF) framework for multi-modal medical data retrieval. PGF models the subjects' relationships in single modalities using the directed propagation graphs, and then fuses the graphs into a single graph by summing up the edge weights. Our proposed PGF method could reduce the large inter-modality and inter-subject variations, and can be solved efficiently using the PageRank algorithm. We test the proposed method on a public medical database with 331 subjects using features extracted from two imaging modalities, PET and MRI. The preliminary results show that our PGF method could enhance multi-modal retrieval and modestly outperform the state-of-the-art single-modal and multi-modal retrieval methods.**

I. Introduction

Medical content-based retrieval (MCBR) is developing rapidly with the advancement of database, computer vision and medical informatics. MCBR has many applications, such as large data management, clinical training and education [1, 2]. Most importantly, it allows us to access a number of pre-diagnosed patient datasets to assist diagnosis and support clinical decisions. Many MCBR methods have been proposed [3–10]. However, these studies mainly focused on single modal data or features, such as High Resolution Computed Tomography (HRCT) [3], Positron Emission Tomography (PET) [4–6], Single Photon Emission Computed Tomography (SPECT) [7], Magnetic Resonance Imaging (MRI) [8, 9], and functional MRI (fMRI) [10].

Recently, multi-modal data are gaining more attention in MCBR since they could provide more insights of the diseases and complement the deficiencies of single modalities [11–14]. A number of multi-modal data fusion methods have been proposed and can be roughly classified into two groups. The first group of methods focuses on selecting or learning the representative features from the data. The most simple and straightforward workflow of these methods is to concatenate features extracted from individual modalities into a high-dimensional vector, and then reduce the dimensions by selecting a subset of features using feature selection methods, such as T-test [15, 16], SVM [17, 18], Elastic Net [19, 20], and the combination of multiple methods [21, 22]. However, the distances between two subjects in feature spaces of different modalities are not directly comparable, and such variations in distances cannot be eliminated by the feature selection methods. The second group is the multi-modal embedding (ME) methods, which are based on manifold learning. They can identify the local geometric structures of subjects across multiple feature spaces and then integrate the local structures in an aligned feature space by preserving the geometric relationships. Several ME methods, such as Multi-view Spectral Embedding (MSE) [23], Supervised Multi-view Spectral Embedding (SMSE) [24], Co-neighbor Multi-view Spectral Embedding (CMSE) [25] and Multi-view Local Linear Embedding (MLLE) [26], have been applied in medical image retrieval. These ME methods could reduce the inter-modality variations. However, the variations among the different query subjects put another bottleneck on the retrieval performance, as current ME methods could not evaluate the query online to customize the multi-modal retrieval strategy.

To further reduce the inter-subject variations in multi-modal data retrieval, in this study, we propose a novel Propagation Graph Fusion (PGF) framework based on the recent query specific fusion (QSF) method [27]. PGF is an unsupervised method, which requires no prior knowledge of the features or the query subjects. The features are first extracted from the multi-modal data, and PGF constructs a network for each feature space by modeling the subjects as nodes and then establishes the edges between the nodes based on the consistency of their neighborhoods. These edges preserve the geometric correlations in each feature space. The most important advantage of PGF is that it is adaptive to the queries. For a given query subject, PGF can generate a query-centric propagation graph which reflects the affinity of the query to its neighboring subjects, then fuse the graphs by summing up the edge weights, and finally rank the subjects according to their equilibrium state probabilities.

We conducted two experiments to validate the proposed PGF on a public medical database with 331 multi-modal neuroimaging datasets. The preliminary results show that PGF achieved a modest improvement over the state-of-the-art multi-modal retrieval methods.

II. Methods

A. Neuroimaging Database and Pre-processing

Data used in the preparation of this research were obtained from the Alzheimer's Disease Neuroimaging Initiative (ADNI) database. The primary goal of ADNI has been to test whether serial MRI, PET, other biological markers, and clinical and neuropsychological assessment can be combined to measure the progression of Mild Cognitive Impairment (MCI) and early Alzheimer's Disease (AD). The identification of sensitive and specific markers of very early AD progression is intended to aid researchers and clinicians to develop new treatments and monitor their effectiveness, as well as lessen the time and cost of clinical trials. For up-to-date information, see www.adni-info.org.

Totally 331 subjects were selected from the ADNI baseline cohort, including 77 cognitive normal (CN), 169 MCI and 85 AD subjects. For each subject, we acquired a T1-weighted volume on a 1.5 Tesla MR scanner and a *2-[18F]fluoro-2-deoxy-d-glucose* (FDG) - PET volume. All these 3D MRI and PET volumes were checked and corrected according to the ADNI pre-processing protocols [28, 29]. The PET volumes were linearly registered to the corresponding MRI volumes using FSL FLIRT [30]. We further performed elastic registration on MRI to the ICBM_152 template [31] using the Image Registration Toolkit (IRTK) [32] and applied the resulting registration coefficients to warp PET volumes into the same ICBM_152 template. The brain volumes in the registered PET and MRI were parcellated into 83 brain functional regions, using the multi-atlas propagation with enhanced registration (MAPER) approach [33].

B. Multi-modal Feature Extraction

To reduce the computational complexity, local region of interest (ROI) measurements from the multiple imaging data were used as basic input features, instead of taking the raw voxels of 3D imaging data as features. We extracted four types of features from the data in total, with two features from PET and two features from MRI. Fig.1 illustrates the pipeline of data pre-processing and feature extraction used in this study.

For PET data, we first estimated the voxel cerebral metabolic rate of glucose consumption (CMRGlc) parameters based on raw uptake values and then normalized the parameters using the mean value of the cerebellum, same as in [21, 34]. The regional CMRGlc parameters are simple and effective in capturing the brain hypo-metabolism patterns; therefore we used the CMRGlc values of the 83 functional regions as the first PET feature. The second PET feature was the lesion-centric feature derived by the Difference-of-Gaussian (DoG) operator [35, 36], for it could not only capture the scale and location of lesions in brain, but also quantize the lesion metabolism rate and contract to the non-lesion parts.

For MRI data, we extracted the grey matter volume from 83 brain regions as the first feature and further normalized it by the volume of the whole brain mask [37, 38]. To measure the effects of cortical atrophy on brain shapes, we further extracted the regional convex hull feature [18, 38] in addition to the grey matter volume. The convex hull feature had two components, convexity and solidity, which were defined as the ratio of the convex hull surface area to the regional surface area and ratio of the convex hull volume to the regional volume, respectively.

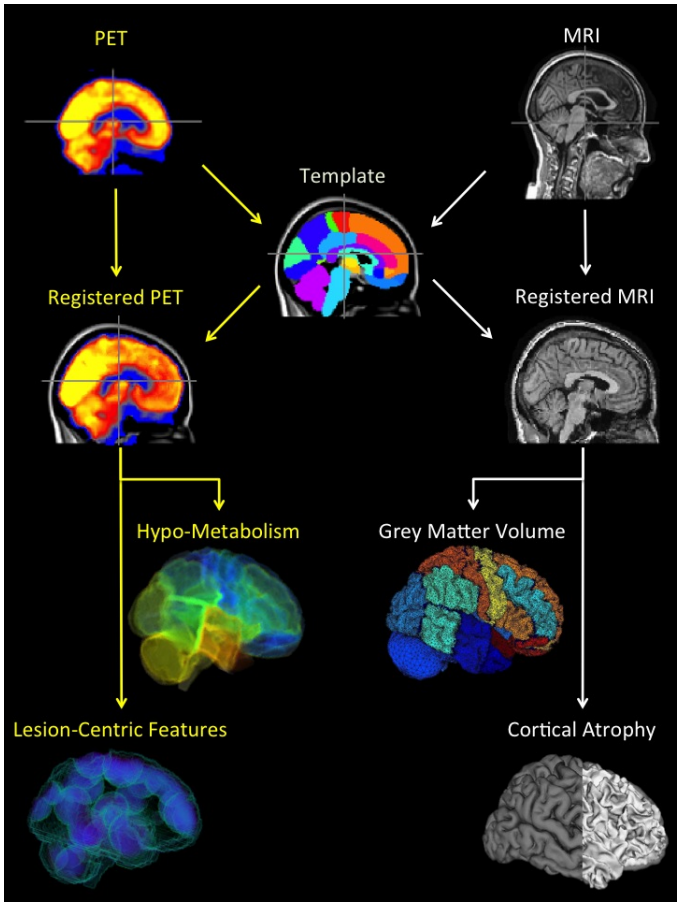

Fig. 1. Data Pre-processing and feature extraction. The brain images are generated using 3D Slicer (V4.3) [39] and BrainVisa (V4.4) [40]

C. Propagation Graph Construction

Given that we have extracted N_v features from N_d subjects in the database ($N_v = 4$, $N_d = 331$ in this study), we could use $x_i^{(n)}$ to represent the feature of the i^{th} subject in the n^{th} feature space. To preserve the local geometric relationships between subjects in each feature space, we built the local neighborhood for each subject in each feature space as $X_i^{(n)} = \left\{x_i^{(n)}, x_{i_1}^{(n)}, \ldots, x_{i_k}^{(n)}\right\}$, where $x_{i_1}^{(n)}, \ldots, x_{i_k}^{(n)}$ are the k nearest neighbors of $x_i^{(n)}$ based on standard Euclidean distance. We further modeled each subject as a node and then establish the edges between them, where the Jaccard coefficients of their neighborhoods were used as the edge weights, as in (1):

$$w(x_i^{(n)}, x_j^{(n)}) = \frac{|X_i^{(n)} \cup X_j^{(n)}|}{|X_i^{(n)} \cap X_j^{(n)}|} \tag{1}$$

The edges formed a network connecting the subjects to each other, and the weights of the edges could reflect the affinity of

the connected subjects. Note that we used Jaccard coefficients instead of distances to construct the neighborhood, because the distance measurements in different feature spaces were not directly comparable. This could also eliminate the potential bias if one less-discriminating feature dominates the retrieval.

PGF applied this procedure to each given query subject, x_q, together with all the subjects in the database, to generate the network, which centered at x_q. We then considered x_q as the source, and let it propagate along all the possible paths in the network and measure the network flow passing through each node. The propagation started from x_q's k nearest neighbors in the n^{th} feature space, $x_{q_1}^{(n)}, \ldots, x_{q_k}^{(n)}$, and continued until no more nodes could be visited. If there was a path connecting the query to a node, then the relevance of the query and the node was proportional to the sum of weights over the path, since the weights reflected the affinity of the query and the subjects. Taking into account this damping effect, we then updated the edge weights for x_q as in (2):

$$w_q^{(n)}(x_i^{(n)}, x_j^{(n)}) = \alpha^{t_q(x_i^{(n)}, x_j^{(n)})} \cdot w(x_i^{(n)}, x_j^{(n)}) \qquad (2)$$

where α is a propagation rate tuning the damping effect, and $t_q(x_i^{(n)}, x_j^{(n)})$ is the number of iterations to reach the edge $(x_i^{(n)}, x_j^{(n)})$. If an edge was visited multiple times, we selected the smallest t_q for it to maximize the flow capacity.

The updated weights were saved in a propagation graph, $G_q^{(n)} = \left(V_q^{(n)}, E_q^{(n)}, w_q^{(n)}\right)$, where V is the set of visited nodes, E is the set of visited edges, and w are the weights of E. The propagation graphs might have different sizes and structures, as many edges might not be visited. Fig.2(a) shows a simple example of propagation graph construction based on 2 nearest neighbors. The network flow starts from the query to its nearest neighbors in the first iteration and then propagates to other nodes alone the possible paths in the following iterations. The circles represent the subjects that have been visited by the query, and different sizes reflect the subject's relevance to the query. The edges show the propagation direction of the flow. In this example, the propagation stops after 2 iterations. However, there are still several subjects unvisited.

D. Graph Fusion

For each query, a group of graphs, $G_q^{(1)}, G_q^{(2)}, \ldots, G_q^{(N_v)}$, could be obtained. We fused these graphs by summing them up into a single graph $G_q = (V_q, E_q, w_q)$, where $V_q = \cup_{N_v} V_q^{(n)}$, $E_q = \cup_{N_v} E_q^{(n)}$, and $w_q(i,j) = \sum_{N_v} w_q^{(n)}(i,j)$ with $w_q^{(n)}(i,j) = 0$ if $(i,j) \notin E_q^{(n)}$. After fusion, we defined a $|V| \times |V|$ affinity matrix A_q for the query, as in (3):

$$A_q(i,j) = \frac{w_q(i,j))}{\sum_{l=|V|} w_q(i,l)} \qquad (3)$$

The values in A indicate the subjects connectivity to the query. Considering A as a transition matrix, there exists an equilibrium state where the probabilities over the nodes to be visited by the query become stable. The probability distribution then can be used as a good relevance estimate to rank the retrieval results. In this study, the PageRank algorithm was employed to derive the equilibrium distributions over the subjects, same as in [27].

Fig.2(b) shows an example of fusing two graphs. Both graphs are derived for the same query, but from different feature spaces as demonstrated by different colors. The circle size is proportional to the edge weights of the path connecting the node and the query. In this example, node i and node j have been included in both graphs, therefore, their relevance measurements become larger in the fused graph and other nodes remain the same as in a single graph.

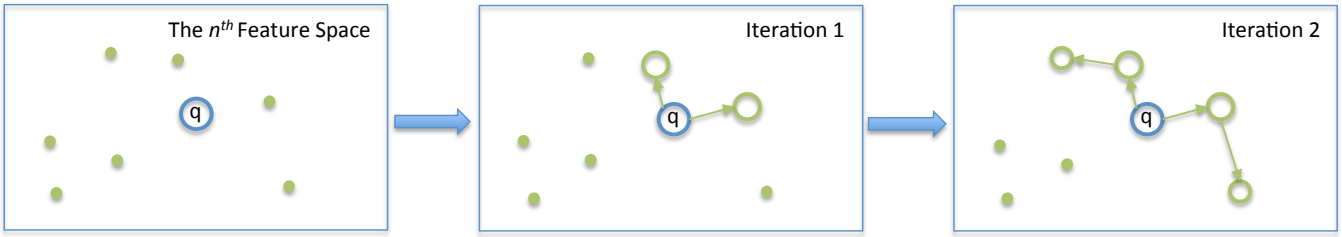

(a). An example of diffusion graph construction, where q is the query; the dots and circles are the subjects in the database.

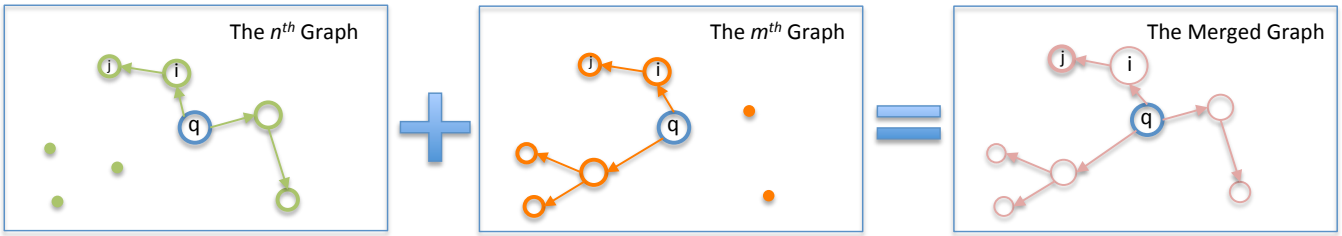

(b). An example of graph fusion, where two graphs derived from different feature spaces are merged.

Fig. 2. The illustration of basic propagation graph construction and fusion.

III. Experiments

In this study, we tested the proposed PGF methods on the dataset described in Section II-A. The dataset was divided into three groups according to the subjects' diagnoses, *i.e.*, cognitive normal (CN), mild cognitive impairment (MCI), and Alzheimer's disease (AD). The retrieval performances on all three groups were evaluated, as well as the average retrieval performance over the entire dataset. We carried out two retrieval experiments. The first experiment focused on single modal data and features, *i.e.*, 1) the regional average metabolism rate (*CMRGlc*), 2) the lesion-centric features derived by DoG operator (*DoG*), 3) the regional grey matter volume (*Grey Matter*), and 4) the brain atrophy features captured by convex hull (*Convex*). The retrieval performances of individual features were used as baselines to validate the effectiveness of multi-modal retrieval methods. The other experiment was conducted on multi-modal data using multi-modal retrieval methods, including *Concatenation*, *Elastic Net*, *MSE* and the proposed *PGF*.

A. Performance Evaluation

For all the methods, we adopted the query-by-example paradigm for retrieval and employed the leave-one-out cross-validation strategy. The performance was evaluated using the modified Mean Average Precision (MAP) [21, 22]. The number of relevant results was set to 5 for all methods. MCI is always considered as a pre-symptomatic status of AD, conferring a high conversion rate to AD. Taking into consideration the close correlation of MCI and AD, we used the following relevance criteria to compute MAP, as shown in Table I.

TABLE I
THE RELEVANCE CRITERIA USED IN COMPUTING THE MAPS (%).

	CN	MCI	AD
CN	1	0.25	0
MCI	0.25	1	0.25
AD	0	0.25	1

The number of nearest neighbors was set as $k = 4$, and the propagation parameter was set as $\alpha = 0.1$ for PGF according to grid search. Other hyper-parameters for these methods were optimized through random search [41].

B. Results

Table II shows the comparison of the results obtained using single-modal features. The best performance for each subject group is highlighted in each row. In general, MRI features work better than PET features in characterizing AD and MCI, especially the Convex feature achieved the best retrieval result at 77.8% for MCI, 53.9% for AD, and 65.5% for three groups combined. The best result for CN is obtained by Grey Matter volume at 53.7%. These results imply that AD and MCI might have a marked effect on brain atrophy patterns, but less effect on the metabolism rates.

TABLE II
THE RETRIEVAL PERFORMANCES OF CN, MCI AND AD USING SINGLE PET AND MRI FEATURES, EVALUATED IN $MAP \pm STD$ (%).

	CMRGlc	DoG	Grey Matter	Convex
CN	51.9±13.4	53.1±13.9	**53.7±13.0**	51.3±13.8
MCI	75.4±11.7	74.9±12.0	76.9±11.6	**77.8±12.1**
AD	49.0±12.9	51.7±13.2	47.3±11.8	**53.9±13.5**
Average	63.2±13.9	63.9±14.0	63.9±13.7	**65.5±14.2**

TABLE III
THE RETRIEVAL PERFORMANCES OF CN, MCI AND AD USING MULTI-MODAL FEATURES, EVALUATED IN $MAP \pm STD$ (%)

	Concatenation	Elastic Net	MSE	PGF
CN	52.7±13.8	58.1±5.6	59.6±6.4	**73.5±5.5**
MCI	77.4±12.0	82.6±5.1	82.5±6.0	**84.9±4.8**
AD	54.3±13.2	62.7±5.2	64.1±5.6	**68.8±6.0**
Average	65.7±14.1	71.8±12.2	72.4±12.3	**78.1±11.4**

Table III shows retrieval performances of different multi-modal retrieval methods. The basic concatenation method works slightly better than the best single-modal feature. Elastic Net is further applied to the concatenated data to select the most discriminating features, and it improves the retrieval of CN by 5.4%, MCI by 5.2%, AD by 8.4% and merged group by 6.1%. Note that Elastic Net is a supervised method, as it requires the label information of the subjects to select the feature. MSE has comparable performance with Elastic Net, and its retrieval performance on CN and AD are slightly better than Elastic Net. PGF achieved the best results on all groups with an average mean average precision of 78.1%. In particular, it has a dramatic good performance on CN at 73.5%, which is 20.8% higher than concatenation method, 15.4% higher than Elastic Net, and 13.9% higher than MSE.

IV. Conclusions

In this study, we proposed a Propagation Graph Fusion (PGF) framework for multi-modal medical content-based retrieval. Multi-modal data could complement the deficiencies of single-modal data in retrieval, and our PGF could further enhance the retrieval by adaptively reshaping the connections between subjects in the different feature spaces and fusing them to retrieve more reliable subjects. PGF is an unsupervised method requiring no prior knowledge. Compared to the state-of-the-art single-modal and multi-modal retrieval methods based on the experiments on the same database, PGF achieved better overall performance than other methods and showed a great potential in multi-modal retrieval.

Acknowledgment

This work was supported in part by ARC, AADRF, NIH NA-MIC (U54EB005149) and NAC (P41EB015902).

References

[1] H. Müller, N. Michoux, D. Bandon, and A. Geissbuhler, "A Review of Content-Based Image Retrieval Systems in

Medical Applications—Clinical Benefits and Future Directions," *International Journal of Medical Informatics*, vol. 73, no. 1, pp. 1–23, 2004.

[2] W. Cai, J. Kim, and D. Feng, "Content-Based Medical Image Retrieval," in *Biomedical Information Technology*, D. Feng, Ed. Elsevier, 2008, ch. 4, pp. 83–113.

[3] A. Foncubierta-Rodríguez, A. Depeursinge, and H. Müller, "Using Multiscale Visual Words for Lung Texture Classification and Retrieval," in *Medical Content-Based Retrieval for Clinical Decision Support*, ser. Lecture Notes in Computer Science, 2012, vol. 7075, pp. 69–79.

[4] W. Cai, D. Feng, and R. Fulton, "Content-based Retrieval of Dynamic PET Functional Images," *Information Technology in Biomedicine, IEEE Transactions on*, vol. 4, no. 2, pp. 152–158, 2000.

[5] W. Cai, S. Liu, L. Wen, S. Eberl, M. J. Fulham, and D. Feng, "3D Neurological Image Retrieval with Localized Pathology-Centric CMRGlc Patterns," in *Image Processing (ICIP), 17th IEEE International Conference on*, 2010, pp. 3201–3204.

[6] S. Liu, W. Cai, L. Wen, S. Eberl, M. J. Fulham, and D. Feng, "Localized Functional Neuroimaging Retrieval using 3D Discrete Curvelet Transform," in *Biomedical Imaging: From Nano to Macro (ISBI), 2011 IEEE International Symposium on*. IEEE, 2011, pp. 1877–1880.

[7] J. Ramírez, J. Górriz, M. López, D. Salas-Gonzalez, I. Álvarez, F. Segovia, and C. Puntonet, "Early Detection of the Alzheimer Disease Combining Feature Selection and Kernel Machines," in *Advances in Neuro-Information Processing*, ser. Lecture Notes in Computer Science, 2009, vol. 5507, pp. 410–417.

[8] D. Unay, A. Ekin, and R. Jasinschi, "Local Structure-Based Region-of-Interest Retrieval in Brain MR Images," *Information Technology in Biomedicine, IEEE Transactions on*, vol. 14, no. 4, pp. 897–903, 2010.

[9] S. Liu, W. Cai, L. Wen, and D. Feng, "Neuroimaging Biomarker based Prediction of Alzheimer's Disease Severity with Optimized Graph Construction," in *Biomedical Imaging: From Nano to Macro (ISBI), IEEE International Symposium on*, 2013, pp. 1324–1327.

[10] R. L. Buckner, W. Koutstaal, D. L. Schacter, A. D. Wagner, and B. R. Rosen, "Functional–Anatomic Study of Episodic Retrieval Using fMRI: I. Retrieval Effort versus Retrieval Success," *NeuroImage*, vol. 7, no. 3, pp. 151 – 162, 1998.

[11] J. Kim, L. Constantinescu, W. Cai, and D. Feng, "Content-based Dual-Modality Biomedical Data Retrieval using Co-Aligned Functional and Anatomical Features," in *Content-based Image Retrieval for Biomedical Image Archives: Achievements, Problems, and Prospects - MICCAI 2007 Workshop on*, 2007, pp. 45–52.

[12] S. Liu, W. Cai, Y. Song, S. Pujol, R. Kikinis, and D. Feng, "A Bag of Semantic Words Model for Medical Content-based Retrieval," in *Medical Content-based Retrieval for Clinical Decision Support (MCBR-CDS), 2013 4th Workshop on*, T. Syeda-Mohmood, H. Greenspan, and A. Madahushi, Eds. IBM Press, 2013, pp. 1–8.

[13] A. Kumar, J. Kim, W. Cai, M. Fulham, and D. Feng, "Content-Based Medical Image Retrieval: A Survey of Applications to Multidimensional and Multimodality Data," *Journal of Digital Imaging*, vol. 26, no. 6, pp. 1025–1039, 2013.

[14] S. Q. Liu, S. Liu, W. Cai, S. Pujol, R. Kikinis, and D. Feng, "Early Diagnosis of Alzhemer's Disease with Deep Learning," in *Biomedical Imaging: From Nano to Macro (ISBI), 2014 IEEE International Symposium on*. IEEE, 2014, pp. 1015–1018.

[15] D. J. Schuirmann, "A Comparison of the Two One-Sided Tests Procedure and the Power Approach for Assessing the Equivalence of Average Bioavailability," *Journal of Pharmacokinetics and Biopharmaceutics*, vol. 15, no. 6, pp. 657–680, 1987.

[16] S. Liu, W. Cai, L. Wen, S. Eberl, M. J. Fulham, and D. Feng, "Generalized Regional Disorder-Sensitive-Weighting Scheme for 3D Neuroimaging Retrieval," in *Engineering in Medicine and Biology Society (EMBC), 2011 Annual International Conference of the IEEE*. IEEE, 2011, pp. 7009–7012.

[17] L. Zhou, L. Wang, L. Liu, P. Ogunbona, and D. Shen, "Support Vector Machines for Neuroimage Analysis: Interpretation from Discrimination," in *Support Vector Machines Applications*, 2014, pp. 191–220.

[18] S. Liu, W. Cai, Y. Song, S. Pujol, R. Kikinis, L. Wen, and D. Feng, "Localized Sparse Code Gradient in Alzheimer's Disease Staging," in *Engineering in Medicine and Biology Society (EMBC), Annual International Conference of the IEEE*, 2013, pp. 5398–5401.

[19] H. Zou and T. Hastie, "Regularization and Variable Selection via the Elastic Net," *Journal of the Royal Statistical Society: Series B (Statistical Methodology)*, vol. 67, no. 2, pp. 301–320, 2005.

[20] L. Shen, S. Kim, Y. Qi, M. Inlow, S. Swaminathan, K. Nho, J. Wan, S. Risacher, L. Shaw, J. Trojanowski, M. Weiner, and A. Saykin, "Identifying Neuroimaging and Proteomic Biomarkers for MCI and AD via the Elastic Net," in *Multimodal Brain Image Analysis - MBIA2011*, ser. Lecture Notes in Computer Science, 2011, vol. 7012, pp. 27–34.

[21] S. Liu, W. Cai, L. Wen, and D. Feng, "Multi-Channel Brain Atrophy Pattern Analysis in Neuroimaging Retrieval," in *Biomedical Imaging: From Nano to Macro (ISBI), IEEE International Symposium on*, 2013, pp. 206–209.

[22] S. Liu, W. Cai, L. Wen, D. D. Feng, S. Pujol, R. Kikinis, M. J. Fulham, and S. Eberl, "Multi-Channel Neurodegenerative Pattern Analysis and Its Application in Alzheimer's Disease Characterization," *Computerized Medical Imaging and Graphics*, 2014.

[23] T. Xia, D. Tao, T. Mei, and Y. Zhang, "Multiview Spectral Embedding," *Systems, Man, and Cybernetics, Part B: Cybernetics, IEEE Transactions on*, vol. 40, no. 6, pp.

1438 – 1446, 2010.

[24] S. Liu, L. Zhang, W. Cai, Y. Song, Z. Wang, L. Wen, and D. Feng, "A Supervised Multiview Spectral Embedding Method for Neuroimaging Classification," in *Image Processing (ICIP), 20th IEEE International Conference on*, 2013, pp. 601–605.

[25] H. Che, S. Liu, W. Cai, S. Pujol, R. Kikinis, and D. Feng, "Co-neighbor Multi-View Spectral Embedding for Medical Content-based Retrieval," in *Biomedical Imaging: From Nano to Macro (ISBI), IEEE International Symposium on*, 2014, pp. 911–914.

[26] H. Shen, D. Tao, and D. Ma, "Multiview Locally Linear Embedding for Effective Medical Image Retrieval," *PLoS ONE*, vol. 8, no. 12, p. e82409, 2013.

[27] S. Zhang, M. Yang, T. Cour, K. Yu, and D. Metaxas, "Query Specific Fusion for Image Retrieval," in *Computer Vision – ECCV 2012*, ser. Lecture Notes in Computer Science, 2012, pp. 660–673.

[28] C. R. Jack, M. A. Bernstein, N. C. Fox, P. Thompson, and et al., "The Alzheimer's Disease Neuroimaging Initiative (ADNI): MRI Methods," *Journal of Magnetic Resonance Imaging (JMRI)*, vol. 27, no. 4, pp. 685–691, 2008.

[29] W. J. Jagust, D. Bandy, K. Chen, N. L. Foster, and et al., "The Alzheimer's Disease Neuroimaging Initiative Positron Emission Tomography Core," *Alzheimer's & Dementia*, vol. 6, no. 3, pp. 221 – 229, 2010.

[30] M. Jenkinson, P. Bannister, M. Brady, and S. Smith, "Improved Optimization for the Robust and Accurate Linear Registration and Motion Correction of Brain Images," *NeuroImage*, vol. 17, no. 2, pp. 825 – 841, 2002.

[31] J. Mazziotta, A. Toga, A. Evans, P. Fox, J. Lancaster, K. Zilles, and et al., "A Probabilistic Atlas and Reference System for the Human Brain: International Consortium for Brain Mapping (ICBM)," *Philosophical Transactions of the Royal Society of London. Series B: Biological Sciences*, vol. 356, no. 1412, pp. 1293–1322, 2001.

[32] J. A. Schnabel, D. Rueckert, M. Quist, J. M. Blackall, A. Castellano-Smith, T. Hartkens, G. P. Penney, W. A. Hall, and et al., "A Generic Framework for Non-rigid Registration Based on Non-uniform Multi-level Free-Form Deformations," in *Medical Image Computing and Computer-Assisted Intervention - MICCAI 2001*, ser. Lecture Notes in Computer Science, 2001, vol. 2208, pp. 573–581.

[33] R. A. Heckemann, S. Keihaninejad, P. Aljabar, K. R. Gray, C. Nielsen, D. Rueckert, J. V. Hajnal, and A. Hammers, "Automatic Morphometry in Alzheimer's Disease and Mild Cognitive Impairment," *NeuroImage*, vol. 56, no. 4, pp. 2024 – 2037, 2011.

[34] S. Liu, W. Cai, L. Wen, S. Eberl, M. J. Fulham, and D. Feng, "A Robust Volumetric Feature Extraction Approach for 3D Neuroimaging Retrieval," in *Engineering in Medicine and Biology Society (EMBC), Annual International Conference of the IEEE*, 2010, pp. 5657–5660.

[35] W. Cai, S. Liu, Y. Song, S. Pujol, R. Kikinis, and D. Feng, "A 3D Difference of Gaussian based Lesion Detector for Brain PET," in *Biomedical Imaging: From Nano to Macro (ISBI), IEEE International Symposium on*, 2014, pp. 677–680.

[36] W. Cai, F. Zhang, Y. Song, S. Liu, L. Wen, S. Eberl, M. J. Fulham, and D. Feng, "Automated Feedback Extraction for Medical Imaging Retrieval," in *Biomedical Imaging: From Nano to Macro (ISBI), IEEE International Symposium on*, 2014, pp. 907–910.

[37] S. Klöppel, C. M. Stonnington, C. Chu, B. Draganski, R. I. Scahill, J. D. Rohrer, N. C. Fox, C. R. Jack, J. Ashburner, and R. S. J. Frackowiak, "Automatic Classification of MR Scans in Alzheimer's Disease," *Brain*, vol. 131, no. 3, pp. 681 – 689, 2008.

[38] S. Liu, Y. Song, W. Cai, S. Pujol, R. Kikinis, X. Wang, and D. Feng, "Multifold Bayesian Kernelization in Alzheimer's Diagnosis," in *Medical Image Computing and Computer-Assisted Intervention – MICCAI 2013*, ser. Lecture Notes in Computer Science, 2013, vol. 8150, pp. 303–310.

[39] A. Fedorov, R. Beichel, J. Kalpathy-Cramer, J. Finet, J.-C. Fillion-Robin, S. Pujol, C. Bauer, D. Jennings, F. Fennessy, M. Sonka, J. Buatti, S. Aylward, J. V. Miller, S. Pieper, and R. Kikinis, "3D Slicer as an Image Computing Platform for the Quantitative Imaging Network," *Magnetic Resonance Imaging*, vol. 30, no. 9, pp. 1323 – 1341, 2012.

[40] D. Geffroy, D. Rivière, I. Denghien, N. Souedet, S. Laguitton, and Y. Cointepas, "BrainVISA: A Complete Software Platform for Neuroimaging," in *Python in Neuroscience Workshop*, 2011.

[41] J. Bergstra and Y. Bengio, "Random Search for Hyper-Parameter Optimization," *Journal of Machine Learning Research (JMLR)*, vol. 13, pp. 281–305, Feb. 2012.